Development of an endoplasmic reticulum-targeting fluorescent probe for the imaging of superoxide anion in living cells

Hua Wei
University of Jinan
Yan Wang
Chemical Technology Academy of Shandong Province
Qingxian Chen
University of Jinan
Yaru Sun
University of Jinan
Baoli Dong (ifp_dongbl@ujn.edu.cn)
University of Jinan

Research Article

Keywords: Fluorescent probe, Endoplasmic reticulum, Superoxide anion, Fluorescent imaging

Posted Date: May 31st, 2022

DOI: https://doi.org/10.21203/rs.3.rs-1675054/v1

Abstract

Superoxide anion ($O_2^{\bullet-}$) is an important reactive oxygen species (ROS), and plays critical roles in biological systems. ER stress has close relation with many metabolic diseases, and could lead to the abnormal production of ROS including $O_2^{\bullet-}$. Herein, we present an ER-targeting probe (**ER-Tf**) for the detection of $O_2^{\bullet-}$ in living cells. The probe **ER-Tf** used triflate as the response site for $O_2^{\bullet-}$, and employed p-methylbenzenesulfonamide as ER-targeting moiety. In response to $O_2^{\bullet-}$, the triflate of the probe **ER-Tf** converted to hydroxyl group, providing strong blue emission under the excitation of ultraviolet light. The probe **ER-Tf** exhibited high sensitivity and selectivity to $O_2^{\bullet-}$. Bioimaging experiments showed that the probe **ER-Tf** can be applied to detect $O_2^{\bullet-}$ at ER, and also demonstrated that rotenone could increase the generation of $O_2^{\bullet-}$ in living cells, while the $O_2^{\bullet-}$ level at ER showed no remarkable change during ferroptosis.

1. Introduction

Superoxide anion($O_2^{\bullet-}$) is a significant reactive oxygen species (ROS), and plays many critical roles in biological system [1–6]. Generally, $O_2^{\bullet-}$ is produced endogenously during cellular respiration, and $O_2^{\bullet-}$ levels are tightly controlled by scavenging enzymes in living organisms and closely related to homeostasis [7]. $O_2^{\bullet-}$ usually serves as a precursor to generate the other ROS including H_2O_2, hydroxyl radical (·OH), hypochlorous acid (HClO),and singlet oxygen ($^1O_2$) [8]. At the same time, $O_2^{\bullet-}$ can also be used as a signal molecule for the redox reaction in biological systems [9, 10]. However, when excess $O_2^{\bullet-}$ is produced, autophagy or apoptotic signaling pathways may be activated, leading to cell death and ultimately to various diseases including atherosclerosis and neurodegenerative diseases [11]. Meanwhile, endoplasmic reticulum (ER) is widely found in various mammal cells, and plays significant roles in the synthesis processes of proteins, lipids, sugars, and also works in maintaining blood glucose levels [12–16]. Many studies have indicated that ER stress is bound up with obesity, insulin resistance and other metabolic diseases, which may lead to abnormal production of reactive oxygen species (ROS), including $O_2^{\bullet-}$ [17,18]. Therefore, development of sensitive and selective method to detect $O_2^{\bullet-}$ at ER is highly significant for intensively studying the pathological role of $O_2^{\bullet-}$ in living systems.

Traditionally, the test methods for the detection of $O_2^{\bullet-}$ chiefly include MS, high performance liquid chromatograph (HPLC) and electron paramagnetic resonance (EPR) [19–22]. Nevertheless, the complex instruments of these methods can damage biological samples and are unsuitable for the real-time detection of $O_2^{\bullet-}$ under the normal physiological conditions. In contrast, fluorescence imaging as an emerging detection technology, has attracted widely attention due to its advantages of high sensitivity, low detection limit, real-time and non-destructive [23–25]. Currently, many fluorescent probes have been developed to detect cellular $O_2^{\bullet-}$ [26–29]. These probes utilized benzothiazoline, catechol, triflate, diphenyl phosphate as the selective recognition sites for $O_2^{\bullet-}$, and studied the endogenous generation of

$O_2^{\bullet-}$ in many organelles including mitochondrial and lysosome. Nevertheless, the fluorescent probes for detecting $O_2^{\bullet-}$ at ER are still very uncommon [30]. Therefore, it is still urgent to construct ER-targeting fluorescence probes for detecting $O_2^{\bullet-}$.

In this work, we have developed a turn-on fluorescent probe (**ER-Tf**) to detect cellular $O_2^{\bullet-}$ at ER (Scheme 1). The probe **ER-Tf** utilized triflate group as a recognition site for $O_2^{\bullet-}$, and utilized p-methylbenzenesulfonamide as an ER-targeting part. **ER-Tf** itself displayed nearly no fluorescence under excitation of ultraviolet light. When **ER-Tf** responded to $O_2^{\bullet-}$, the triflate moiety converted to hydroxyl group, accompanying by the generation of strong blue emission. The probe **ER-Tf** showed the high sensitivity and selectivity to $O_2^{\bullet-}$. In addition, **ER-Tf** can be used as an ER-targeting probe in bioimaging experiments for detecting cellular $O_2^{\bullet-}$ at ER.

2. Experimentation

2.1. Synthesis of Compound ER-Cou

The mixture of 7-hydroxy-2-oxo-2H-chromene-3-carboxylic acid(206mg,1mmol), N-(2-aminoethyl)-4-methylbenzenesulfonamide (214 mg, 1 mmol), HOBt (67.5 mg, 0.5 mmol), EDC (382 mg, 2 mmol), 150 μL diisopropylethylamine (DIEA) in 5 mL DMF was stirred vigorously in a N_2 atmosphere for 5 hours. Then, 10 mL water was slowly added to the solution, and then the solution was extracted it with CH_2Cl_2, washed with H_2O and dried it with sodium sulfate, concentrated in vacuum. The crude product was then purified by the chromatographic column method (CH_2Cl_2: MeOH = 20:1) to provide the compound **ER-Cou** (261 mg, 65%) as a brown solid. ^{1}H NMR (400 MHz, DMSO-d_6) δ 11.09 (s, 1H), 8.72 (m, 2H), 7.83 (d, J = 8.4 Hz, 1H), 7.71 (t, 1H), 7.69 (d, J = 8.0 Hz, 2H), 7.32 (d, J = 8.0 Hz, 2H), 6.90 (dd, 1H), 6.82 (m, 1H), 3.35 (m, 2H), 2.92 (q, 2H), 2.24 (s, 3H). ^{13}C NMR (101 MHz, DMSO-d_6) δ 164.14, 162.18, 161.23, 156.77, 148.52, 142.96, 137.92, 132.50, 129.99, 127.00, 114.82, 113.85, 111.54, 102.26, 42.39, 21.26. HRMS (ESI): m/z cald. for $C_{19}H_{18}N_2O_6S$, $[M + H]^+$ 403.0958, found 403.0966.

2.2 Synthesis of the probe ER-Tf

The mixture of compound **ER-Cou** (201 mg, 0.5 mmol), N-phenyl-bis(trifluoromethanesulfonimide) ($PhN(SO_2CF_3)_2$, 357mg, 1mmol), K_2CO_3 (138mg, 1mmol) in 10 mL THF was stirred for 6 hours. Then, the mixture was concentrated in vacuum and purified by a column chromatography (CH_2Cl_2:MeOH = 20:1), and provided the probe **ER-Tf** as a white solid (141 mg, 53%). ^{1}H NMR (400 MHz, DMSO-d_6) δ 8.85 (s, 1H), 8.72 (t, 1H), 8.21 (d, J = 8.8 Hz, 1H), 7.91 (d, J = 2.0 Hz, 1H), 7.73 (t, 1H), 7.67 (m, 3H), 7.33 (d, J = 8.0 Hz, 2H), 3.35 (m, 2H), 2.95 (q, 2H), 2.24 (s, 3H). ^{13}C NMR (101 MHz, DMSO-d_6) δ 161.32, 159.88, 154.79, 151.95, 146.74, 142.99, 137.94, 132.87, 130.02, 127.02, 120.20, 119.38, 118.93, 110.76, 42.22, 21.23. HRMS (ESI): m/z cald. for $C_{20}H_{17}F_3N_2O_8S_2$, $[M + H]^+$ 535.0451, found 535.0391.

2.3 Cell culture and fluorescence imaging

HeLa cells were obtained from the College of Life Science, Nankai University (Tianjin, China). Hela cells were used to study the properties of **ER-Tf**, the cells were cultured in a medium containing 10% heat-inactivated fetal bovine serum and 1% antibiotics in air at 37°C (5% CO2). Before fluorescence imaging, the HeLa cells were inoculated into a glass cover and cultured for 24 hours to achieve the suitable density. The images were obtained by a Nikon A1R confocal microscope.

1. Fluorescence of imaging exogenous $O_2^{\bullet-}$: 5 μM **ER-Tf** was used to stain Hela cells for 20 min, followed by washing cells with PBS. Then the HeLa cells were incubated with 50 μM $O_2^{\bullet-}$ sulution for 20 min, and subsequently washed with PBS for three times and imaged.
2. Fluorescence of imaging endogenous $O_2^{\bullet-}$: Firstly, the HeLa cells were incubated with 10 μM or 20 μM rotenone for 30 min, or treated with 10 μM erastin for 2h, and then washed with PBS for three times. Whereafter, 5 μM **ER-Tf** was used to stain HeLa cells for another 20 min, and subsequently the cells were washed with PBS for three times and imaged.

3. Results And Discussion

3.1 Synthesis of ER-targeting probe (ER-Tf) for $O_2^{\bullet-}$

In order to meet requirements for the fluorescence imaging of cellular $O_2^{\bullet-}$ at ER, the designed fluorescent probe should structurally contain three units including fluorophore, response site of $O_2^{\bullet-}$ and ER-targeting group. Accordingly, we constructed the ER-targeting fluorescent probe (**ER-Tf**) for detecting cellular $O_2^{\bullet-}$ at ER. In the chemical structure of **ER-Tf** (scheme 1), coumarin group was used as the fluorophore, p-methylsulfonamide acted as an ER-targeting part, and triflate group was selected as a reaction site for the reorganization of $O_2^{\bullet-}$ [30].The synthetic route is revealed in scheme 1, and the chemical structures were characterized by ^{1}H NMR, ^{13}C NMR and HRMS.

3.2. Optical properties of the probe ER-Tf

Firstly, we investigated the absorption spectra of the probe **ER-Tf** treated with or without $O_2^{\bullet-}$. The probe **ER-Tf** showed no significant absorption peak in the visible region in PBS (20 mM, 5% MeOH) (Fig. 1A). However, after 20 μM $O_2^{\bullet-}$ was added to 5μM **ER-Tf** solution, an absorption peak could be clearly found at 405 nm, indicating that the probe **ER-Tf** reacted with $O_2^{\bullet-}$. Under 405 nm excitation, the probe **ER-Tf** showed nearly no fluorescence (Fig. 1B). Upon the introduction of $O_2^{\bullet-}$, the fluorescence peak at 462 nm appeared and increased continuously along with the gradual change of $O_2^{\bullet-}$ concentration from 0 μM to 90 μM (Fig. 1C). Meanwhile, the intensity of the fluorescence at 462 nm displayed the satisfactory linear relationship (R^2 = 0.9909) with $O_2^{\bullet-}$ concentration in the range 5–60 μM, and the detection limit was

calculated to 65 nM (Fig. 1D). In addition, after **ER-Tf** reacted with $O_2^{\bullet-}$, the fluorescence intensity reached the maximum at 462 nm within 7 min (Figure S1). Hence, **ER-Tf** could be used as a sensitive fluorescent probe to detect $O_2^{\bullet-}$.

Whereafter, we assessed the selective property of the probe **ER-Tf** to $O_2^{\bullet-}$. As shown in Fig. 2, the fluorescence spectra of **ER-Tf** showed negligible change in the following the addition of different biologically related species including the other ROS (H_2O_2, ClO^-, etc), reactive nitrogen species, Cys, GSH and a battery of ions. By contrast, when the probe **ER-Tf** was added to 90 μM $O_2^{\bullet-}$, a strong fluorescent peak at 462 nm can be clearly obtained, manifesting that **ER-Tf** had a desirable selectivity to $O_2^{\bullet-}$. Furthermore, **ER-Tf** exhibited excellent fluorescence response to $O_2^{\bullet-}$ at pH 4.0–9.0. Considering that the normal pH at ER is about 7.2 (Figure S2), **ER-Tf** can potentially be used as the selective fluorescent probe for the detection of cellular $O_2^{\bullet-}$ at ER.

The response mechanism to $O_2^{\bullet-}$ of **ER-Tf** was then explored by HRMS test. As shown in the HRMS data of the reaction product between **ER-Tf** with $O_2^{\bullet-}$(Figure S3), besides the peak at 535.0391 corresponding to **ER-Tf** (Cald. for $[M + H]^+$, 535.0451), an obvious peak at 403.0966 and 425.0785, corresponding the compound **ER-Cou** (Cald. for $[M + H]^+$, 403.0958; Cald. for $[M + Na]^+$, 425.0778), indicating that the emissive compound **ER-Cou** was generated after the reaction of **ER-Tf** and $O_2^{\bullet-}$ (Figure S3). We proposed that $O_2^{\bullet-}$ firstly attacked S atom of triflate group, and then peroxytriflate free radical was removed to provide the emissive compound **ER-Cou** by protonation (Scheme 2).

Then, we tried to study the ability of **ER-Tf** to detect $O_2^{\bullet-}$ at ER. The MTT assay showed that **ER-Tf** showed very low cytotoxity below the concentration of 15 μM (Figure S4). When the HeLa cells were only treated with 5 μM **ER-Tf** for 20 min, almost no fluorescence was found under the excitation at 405 nm. Nevertheless, after the cells were firstly incubated with 30 μM or 60 μM $O_2^{\bullet-}$, the bright fluorescence can be found in blue channel (Fig. 3A). It indicated that **ER-Tf** can visualize $O_2^{\bullet-}$ at ER. Besides, the fluorescence intensity of the cells treated with 60 μM $O_2^{\bullet-}$ was more intense than that of the cells incubated with 30 μM $O_2^{\bullet-}$, suggesting that the probe **ER-Tf** could evaluate the concentration of cellular $O_2^{\bullet-}$ (Fig. 3B). Hence, **ER-Tf** could act as a sensitive fluorescent probe to detect $O_2^{\bullet-}$ in living cells.

Subsequently, in order to explore the ER-targeting ability of the probe **ER-Tf**, we selected the commercial ER-specific dye (ER-tracker) as a reference to compare the positioning ability of the probe **ER-Tf.** The specific operation of the experiment was as follows: Firstly, the cells were treated with 5 μM **ER-Tf** and incubated at a constant temperature for 20 min, and then washed off the medium and incubated with 50 μM $O_2^{\bullet-}$, finally treated with 1 μM ER-tracker. Then we observe the positioning of the probe **ER-Tf** under a confocal microscope, the blue channel signal generated by the reaction of **ER-Tf** with $O_2^{\bullet-}$ can better overlap with the red channel signal generated by the ER-tracker, and the Pearson correlation coefficient is

as high as 0.89 (Fig. 4).Therefore, the co-localization experiment showed that **ER-Tf** possessed ER-targeting property.

Then, we assessed the ability of **ER-Tf** to image endogenous $O_2^{\bullet-}$ in living cells. Rotenone, as a mitochondrial electron transport chain complex I inhibitor, which can lead to apoptosis and increase the production of ROS [31]. When HeLa cells were coated with 5μM **ER-Tf** for 20 min, almost no fluorescence was observed in the blue channel (Fig. 5). While HeLa cells were firstly treated with 10 μM or 20μM rotenone for 30 min and then stained with 5 μM **ER-Tf** for 20 min, the bright fluorescence could be found in blue channel. It indicates that HeLa cells produce $O_2^{\bullet-}$ when stimulated by rotenone. In addition, we evaluate the changes of endogenously generated cellular $O_2^{\bullet-}$ during ferroptosis. Erastin is a famous iron ion activator, which can inhibit the uptake of cystine by cystine/glutamate reverse transporter (system XC), and finally lead to ferroptosis. Erastin was employed as an activator to investigate the subtle changes of $O_2^{\bullet-}$ in living cells during ferroptosis [32]. After treatment of HeLa cells with 10 μM erastin for 2 h and then 5μM **ER-Tf** for 20 min, the fluorescence intensity of blue channel showed nearly no change (Fig. 5). It suggests that the $O_2^{\bullet-}$ level at ER showed no remarkable change during ferroptosis. Hence, **ER-Tf** can be used for the fluorescence imaging of endogenously generated $O_2^{\bullet-}$ at ER.

4. Conclusion

We have developed an ER-targeting probe (**ER-Tf**) for the detection of cellular $O_2^{\bullet-}$. **ER-Tf** used triflate group as a recognition site for $O_2^{\bullet-}$, employed p-methylbenzenesulfonamide as an ER-targeting unit. After the response of **ER-Tf** to $O_2^{\bullet-}$, triflate moiety of **ER-Tf** converted to hydroxyl group, providing strong blue emission under the excitation. The probe **ER-Tf** probes exhibited high sensitivity and selectivity to $O_2^{\bullet-}$. The bio-imaging experiments showed the probe **ER-Tf** can be used as an ER-targeting probe to detect cellular $O_2^{\bullet-}$ at ER. Rotenone could increase the generation of $O_2^{\bullet-}$ in living cells, while the $O_2^{\bullet-}$ level at ER showed no remarkable change during ferroptosis.

Declarations

Authors' Contributions

All authors contributed to the study conception and design. Material preparation, data collection and analysis were performed by H. Wei, Y. Wang, Q. Chen, Y. Sun and B. Dong. The first draft of the manuscript was written by H. Wei and B. Dong. All authors read and approved the final manuscript."

Conflicts of interest

The authors declare they have no competing interests

Funding

This work was supported by NSFC (51602127) and the Natural Science Foundation of Shandong Province (ZR2021MB022).

Ethics Declaration statement

Not applicable.

Consent to Participate

Not applicable.

Consent for publication

Not applicable.

Data Availability

All data generated or analysed during this study are included in this published article (and its supplementary information files).

References

1. Finkel T, Holbrook NJ (2000) Oxidants, oxidative stress and the biology of ageing. *Nature 408*:239-247. https://doi. org/10.1038/35041687
2. Thannickal VJ, Fanburg BL (2000) Reactive oxygen species in cell signaling. *Ajp Lung Cell Mol Physiol 279*:1005-1028. https://doi. org/10.1152/ajplung.2000.279.6.L1005
3. Bergamini CM, Gambetti S, Dondi A, Cervellati C (2004) Oxygen, reactive oxygen species and tissue damage. *Curr Pharmaceut Des10*:1611-1626. https://doi. org/10.2174/1381612043384664
4. Wallace DC (1999) Mitochondrial diseases in man and mouse. *Science283*:1482-1488. https://doi. org/10.1126/science.283.5407.1482
5. Nathan C, Cunningham-Bussel A (2013) Beyond oxidative stress: an immunologist's guide to reactive oxygen species. *Nat Rev Immunol 13*:349-361. https://doi.org/10.1038/nri3423
6. Prasad S, Gupta SC, Tyagi AK (2017) Reactive oxygen species (ROS) and cancer: role of antioxidative nutraceuticals. *Canc Lett 387*: 95-105. https://doi. org/ 10.1016/j.canlet.2016.03.042
7. Rahmani H, Ghavamipour F, Sajedi RH (2019) Bioluminescence detection of superoxide anion using aequorin. *Anal Chem 91*:12768-12774. https://doi. org/ 10.1021/acs.analchem.9b02293
8. Turrens JF (2003) Mitochondrial formation of reactive oxygen species. *J Physiol 552*: 335-344. https://doi. org/10.1113/jphysiol.2003.049478
9. Sheng Y, Abreu IA, Cabelli DE, Maroney MJ, Miller AF, Teixeira M, Valentine JS (2014) Superoxide dismutases and superoxide reductases. *Chem Rev114*: 3854-3918. https://doi. org/10.1021/cr4005296

10. Chen Z, Li Q, Sun Q, Chen H, Wang X, Li N, Yin M, Xie Y, Li H, Tang B (2012) Simultaneous determination of reactive oxygen and nitrogen species in mitochondrial compartments of apoptotic HepG2 cells and PC12 cells based on microchip electrophoresis-laser-induced fluorescence. *Anal Chem84*: 4687-4694. https://doi. org/10.1021/ac300255n
11. Qu LL, Li DW, Qin LX, Mu J, Fossey JS, Long YT (2013) Selective and sensitive detection of intracellular $O_2^{\cdot-}$ using Au NPs/cytochrome c as SERS nanosensors. *Anal Chem 85*: 9549-9555. https://doi. org/10.1021/ac401644n
12. Pollard TD, Earnshaw WC, Johnson GT (2017) Cell Biology, third ed., Elsevier, Netherlands.
13. Ellgaard L, Helenius A (2003) Quality control in the endoplasmic reticulum. *Nat Rev Mol Cell Biol 4*: 181-191. https://doi. org/10.1038/nrm1052
14. Görlach A, Klappa P, Kietzmann T (2006) The endoplasmic reticulum: folding, calcium homeostasis, signaling, and redox control. *Antioxidants Redox Signal 8*: 1391-1418. https://doi. org/10.1089/ars.2006.8.1391
15. Sitia R, Braakman I (2003) Quality control in the endoplasmic reticulum protein factory. *Nature 426*: 891-894. https://doi. org/10.1038/nature02262
16. Sano R, Reed JC (2013) ER stress-induced cell death mechanisms. *Biochim Biophys Acta 1833*: 3460-3470. https://doi. org/10.1016/j.bbamcr.2013.06.028
17. Bernales S, McDonald KL, Walter P (2006) Autophagy counterbalances endoplasmic reticulum expansion during the unfolded protein response. *PLoS Biol 4*: e423. https://doi. org/10.1371/journal.pbio.0040423
18. Bernales S, Schuck S, Walter P (2007) Selective autophagy of the endoplasmic reticulum. *Autophagy 3*: 285-287. https://doi. org/10.4161/auto.3930
19. Chen XJ, West AC, Cropek DM, Banta S (2008) Detection of the superoxide radical anion using various alkanethiol monolayers and immobilized cytochrome c. *Anal Chem 80*: 9622-9629. https://doi. org/10.1021/ac800796b
20. Abbas K, Hardy M, Poulhès F, Karoui H, Tordo P, Ouari O, Peyrot F (2014) Detection of superoxide production in stimulated and unstimulated living cells using new cyclic nitrone spin traps. *Free Redical Bio Med71*: 281-290. https://doi.org/10.1016/j.freeradbiomed.2014.03.019
21. Yasui H, Sakurai H(2000) Chemiluminescent detection and imaging of reactive oxygen species in live mouse skin exposed to UVA. *Biochem Biophys Res Commun 269*: 131-136. https://doi.org/10.1006/bbrc.2000.2254
22. Derkus B, Emregul E, Emregul KC (2015) Copper-zinc alloy nanoparticle based enzyme-free superoxide radical sensing on a screen-printed electrode. *Talanta 134*: 206-214. https://doi.org/10.1016/j.talanta.2014.11.003
23. Lakowicz JR (2006) Principles of Fluorescence Spectroscopy, third ed., Springer, New York.
24. Chan J, Dodani SC, Chang CJ (2012) Reaction-based small-molecule fluorescent probes for chemoselective bioimaging. *Nat Chem 4*: 973-984. https://doi. org/ 10.1038/nchem.1500

25. Wang Y, Lu G, Tu Y, Pu S (2021) A Turn-on Fluorescent Probe for the Discrimination of Cys/Hcy and GSH With Dual Emission Signals. *Journal of Fluorescence* 31:599-607 https://doi.org/10.1007/s10895-021-02684-6
26. Chen X, Tian X, Shin I, Yoon J (2011) Fluorescent and luminescent probes for detection of reactive oxygen and nitrogen species. *Chem Soc Rev 40*: 4783-4804. https://doi.org/10.1039/C1CS15037E
27. Cao D, Liu Z, Verwilst P, Koo S, Jangjili P, Kim JS, Lin W (2019) Coumarin-Based Small-Molecule Fluorescent Chemosensors. *Chem Rev 119*: 10403-10519. https://doi. org/10.1021/acs.chemrev.9b00145
28. Kim HM, Cho BR (2015) Small-Molecule Two-Photon Probes for Bioimaging Applications. *Chem Rev 115*, 5014-5055. https://doi. org/10.1021/cr5004425
29. Jiao X, Li Y, Niu J, Xie X, Wang X, Tang B (2018) Small-Molecule Fluorescent Probes for Imaging and Detection of Reactive Oxygen, Nitrogen, and Sulfur Species in Biological Systems. *Anal Chem 90*: 533-555. https://doi. org/10.1021/acs.analchem.7b04234
30. Lu Y, Wang R, Sun Y, Tian M, Dong B (2021) Endoplasmic reticulum-specific fluorescent probe for the two-photon imaging of endogenous superoxide anion ($O_2^{\bullet-}$) in live cells and zebrafishes. *Talanta 225*: 122020. https://doi. org/10.1016/j.talanta.2020.122020
31. Kuwabara WMT, Zhang L, Schuiki I, Curi R, Volchuk A, Alba-Loureiro TC (2015) NADPH oxidase-dependent production of reactive oxygen species induces endoplasmatic reticulum stress in neutrophil-like HL60 cells. *PloS One 10*: e0116410. https://doi.org/10.1371/journal.pone.0116410
32. Dixon SJ, Lemberg KM, Lamprecht MR, Skouta R, Zaitsev EM, Gleason CE, Patel DN, Bauer AJ, Cantley AM, Yang WS, Morrison B, Stockwell BR (2012) Ferroptosis: an iron-dependent form of nonapoptotic cell death. *Cell 149*: 1060-1072. https://doi.org/10.1016/j.cell.2012.03.042

Scheme

Scheme 1 and 2 are available in the Supplementary Files section

Figures

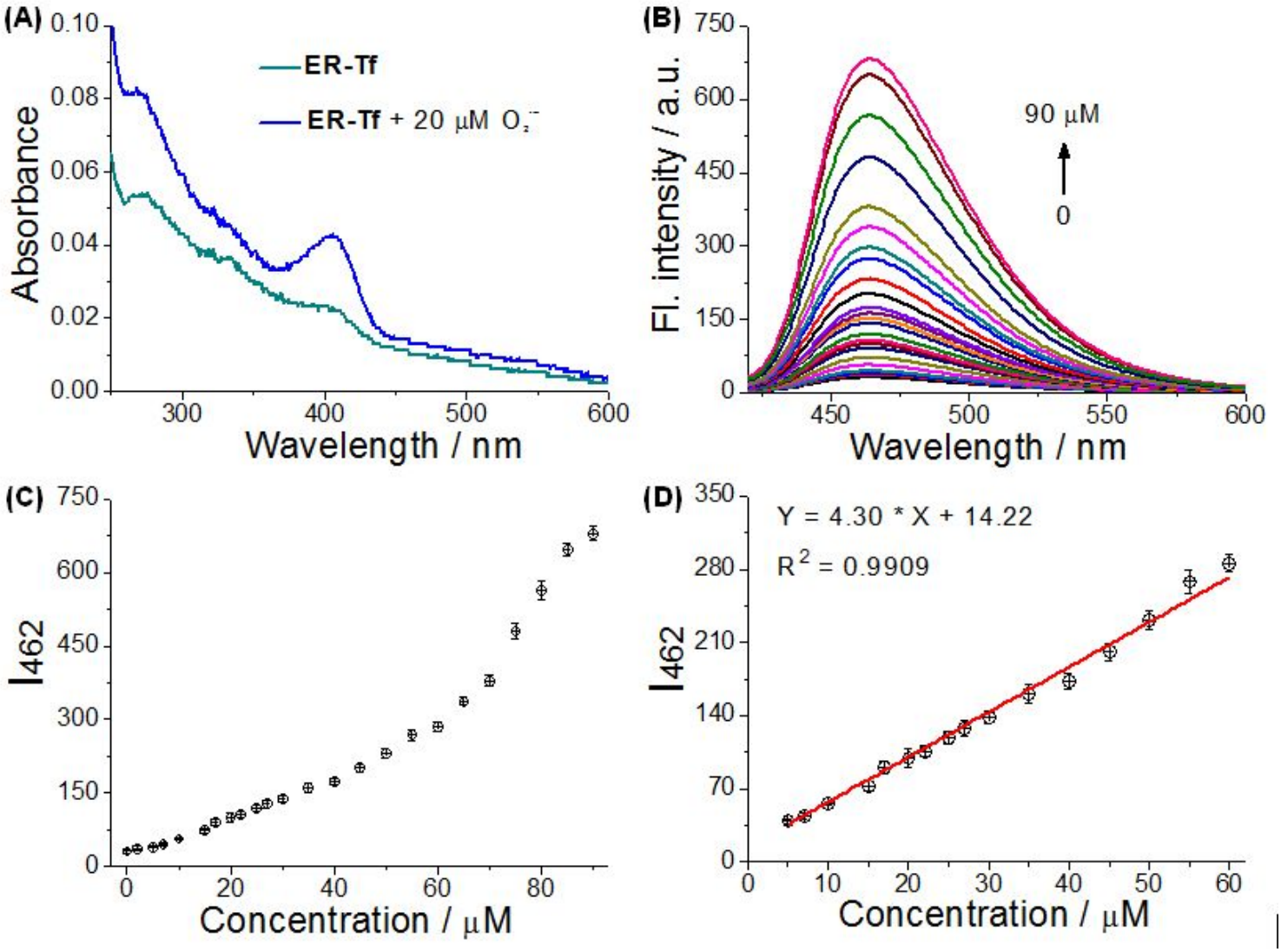

Figure 1

(A) Absorption spectra of 5μM **ER-Tf** in PBS (20mM, pH 7.4, 5% MeOH) in absence and presence of 20 μM $O_2^{\bullet-}$. (B) Fluorescence spectra of 5 μM **ER-Tf** upon addition of 0-90 μM $O_2^{\bullet-}$. (C) Fluorescence intensity at 462 nm of 5 μM **ER-Tf** treated with 0-90 μM $O_2^{\bullet-}$. (D) Linear relationship with $O_2^{\bullet-}$ concentration in the range 5-60μM and fluorescence intensity at 462 nm. λ_{ex} = 405 nm.

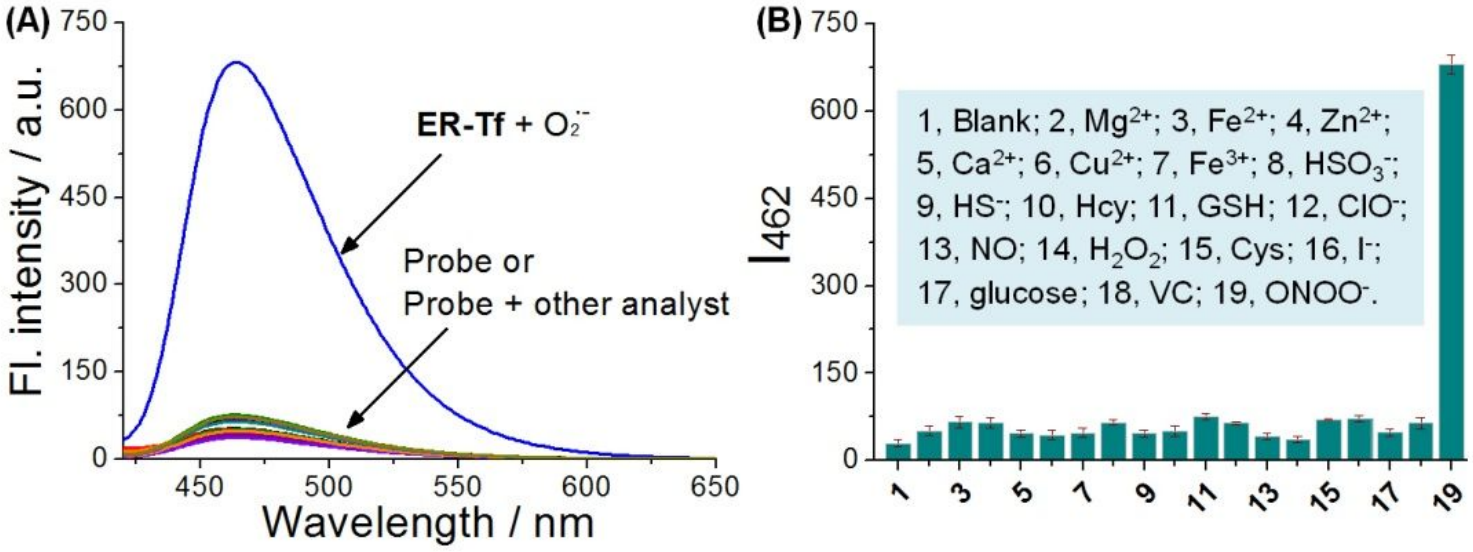

Figure 2

Fluorescence spectra (A) and fluorescent intensity at 462 nm (I_{462}) (B) of 5 μ M **ER-Tf** towards various species. Concentration: GSH, Mg^{2+} and Ca^{2+}: 1 mM; $O_2^{\bullet-}$: 90 μM; other analytes:100 μM. All the data were obtained in PBS (20 mM, pH 7.4, 5% MeOH). λ_{ex} = 405 nm.

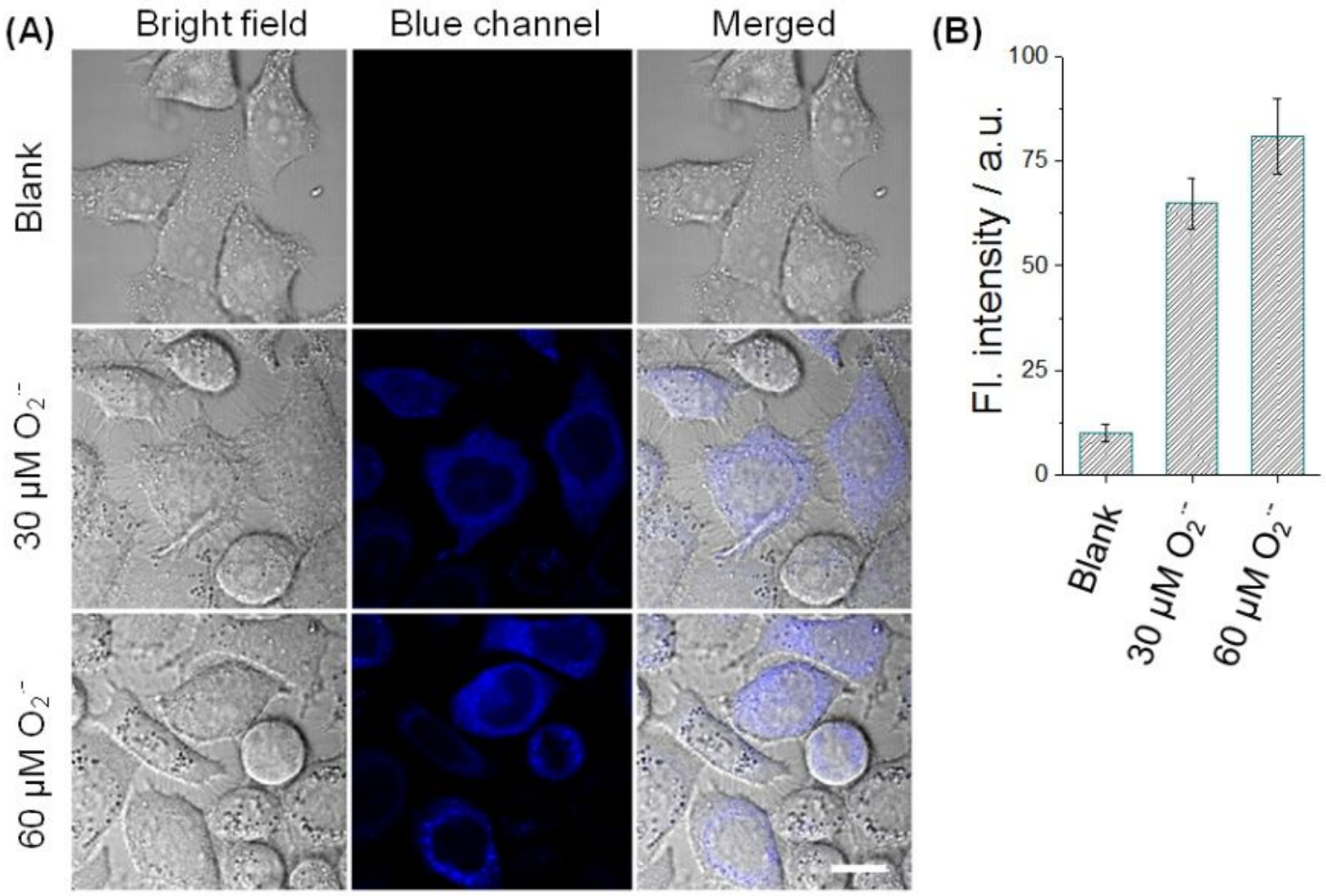

Figure 3

(A) Fluorescence imaging of the HeLa cells stained with 5 μM **ER-Tf** for 20 min and then treated with 30 μM or 60 μM $O_2^{\bullet-}$ for another 20 min. Blue channel: λ_{ex} = 405 nm, λ_{em} = 500-550 nm; Scale bar =10 μm. (B) Quantitative analysis for (A) by Image J.

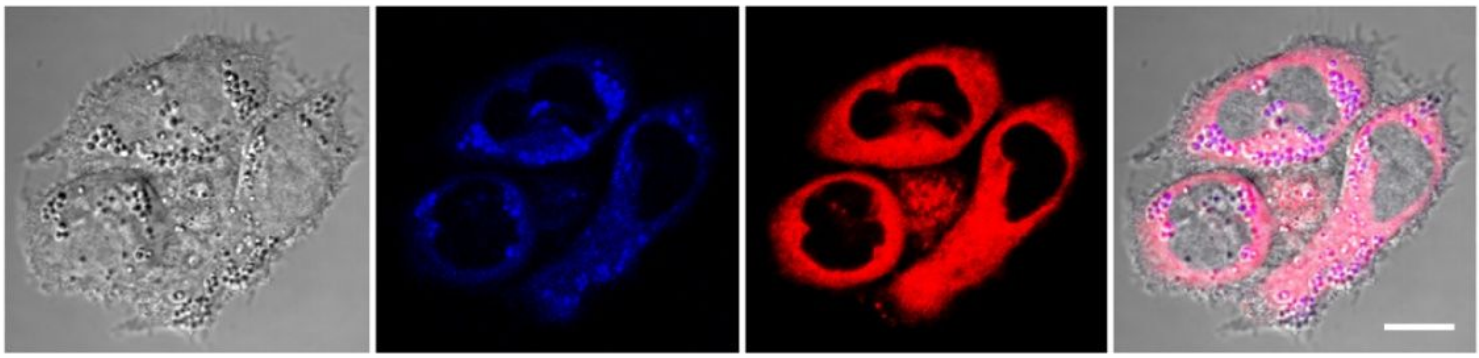

Figure 4

Images of HeLa cells treated with 5 μM **ER-Tf** for 20 min, and treated with 50 μM $O_2^{\bullet-}$ for another 20 min, and then stained with 1 μM ER-tracker for 10 min. Blue channel, λ_{ex} = 405 nm, λ_{em} = 425-475 nm; Red channel: λ_{ex} = 561 nm, λ_{em} = 570-620 nm. Scale bar =10 μm.

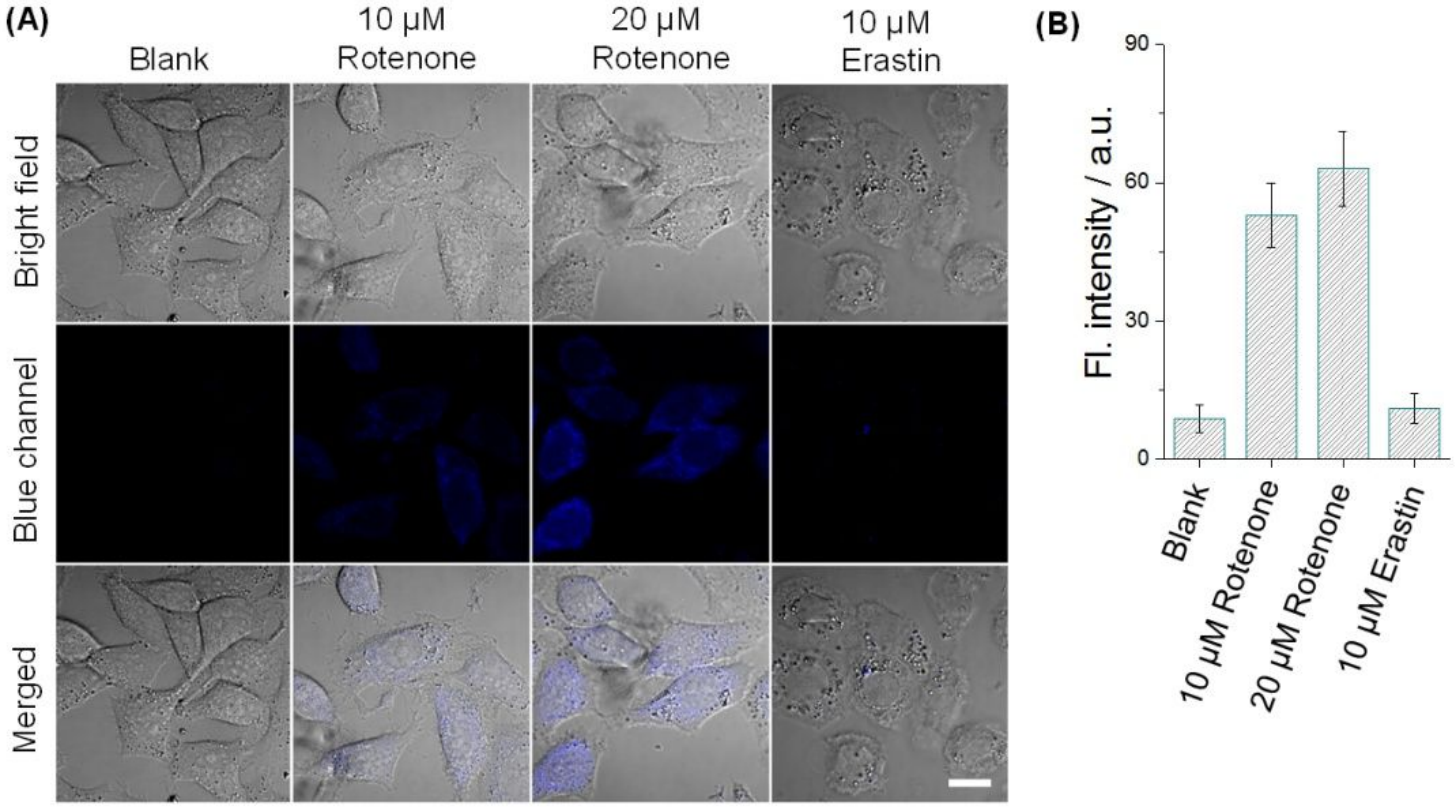

Figure 5

(A) Fluorescence imaging of the HeLa cells with 10 μM or 20 μM rotenone for 30 min, or treated with 10 μM erastin for 2h, and then incubated with 5 μM **ER-Tf** for 20 min. Blue channel: λ_{ex} = 405 nm, λ_{em} = 500-550 nm; Scale bar =10 μm. (B) Quantitative analysis for (A) by Image J.

Supplementary Files

This is a list of supplementary files associated with this preprint. Click to download.

- JFSIDong.docx
- Onlinefloatimage1.png
- Onlinefloatimage4.png